Evidence of Domain Formation in Cardiolipin−Glycerophospholipid Mixed Monolayers. A Thermodynamic and AFM Study

S. Sennato,[†] F. Bordi,[†] C. Cametti,*[,†] C. Coluzza,[†] A. Desideri,[‡] and S. Rufini[‡]

Dipartimento di Fisica, Universita' di Roma "La Sapienza", Piazzale A. Moro 5, I-00185 Rome, Italy, and INFM-CRS SOFT, Unita' di Roma 1, and Dipartimento di Biologia, Universita' di Roma "Tor Vergata", V. Tor Vergata 135, I-00133 Rome, Italy, and INFM, Unita' di Roma 2

Received: April 12, 2005; In Final Form: June 30, 2005

The interaction of the three main components of the mitochondrial membrane, namely cardiolipin, phosphatidylcholine, and phosphatidylethanolamine, has been studied investigating mixed cardiolipin−phosphatidylcholine and cardiolipin−phosphatidylethanolamine monolayers at different cardiolipin molar fractions. The thermodynamic behavior of the mixed monolayers was investigated by means of surface pressure and surface potential measurements, and atomic force microscopy was employed to characterize the morphology of the monolayers. Langmuir isotherms and surface potential curves show a regular behavior with a progressive transition toward the isotherm of the pure component. Positive deviations from ideality in the excess Gibbs energies of mixing suggest the presence of repulsive interactions in both systems. Analysis of partial molecular dipole moment indicates a discontinuity at a definite cardiolipin/phosphatidylethanolamine molar fraction, suggesting the formation of a stoichiometric complex; as a consequence, in mixed cardiolipin−phosphatidylethanolamine monolayers, a phase separation is observed at phosphatidylethanolamine excess. AFM measurements indicate the presence of two domains: one made by phosphatidylethanolamine and the other by a regular arrangement of phosphatidylethanolamine and cardiolipin at a fixed molecular ratio.

1. Introduction

Cardiolipin (CLP), a dimeric anionic phospholipid carrying four acyl chains, is localized almost exclusively in membranes of several eubacteria[1] and in the inner membrane of eukaryotic cell mitochondrion, where it represents the 25−30% of total lipid mass.[2] The presence of cardiolipin in the mitochondrion membrane has been related to the maintenance of the structure of mitochondrial cristae[3] and to the stabilization of different protein complexes.[4] Several purified mitochondrion proteins have been found to contain a distinct number of cardiolipin molecules firmly integrated in their quaternary structure. Furthermore, CLP may also be involved in the promotion of conformational transitions necessary for a catalytic activity due to the spatial sequestering in appropriate patches of the membrane.[5]

So far, no information is available about the lateral organization of mitochondrion and whether different lipid domains coexist. However, indications of the achievement of a specific activity mediated by a CLP spatial organization within the membrane have been recently reported.[6,7] CLP-enriched regions of mitochondrion membrane have been proposed to be the target for different pre-apoptothic proteins, such as t-BID and BAX,[6] and to represent the trigger for the translocation across the mitochondrial membrane.[7]

In eukaryotic cells, plasma membranes are not laterally homogeneous but are organized in domains with distinct lipid and protein compositions.[8] This organization plays an important role in defining specific membrane functions, such as ionic transport, signal transduction, cell growth, and matrix−protein interactions. Recently, evidence of the existence of lipid domains has been also provided for bacteria membrane using a cardiolipin-specific fluorescent dye.[9,10] As well as PE, PC has been reported to be crucial for the topological organization of several bacterial integral proteins, such as lactose[11] and phenylalanine permeases.[12]

Lateral segregation of sphingolipids in Langmuir−Blodgett films made by PC and sphingolipids, similar to ones observed in biological membranes, has been found by using different techniques such as fluorescence,[13] NMR,[14] and atomic force microscopy.[15] To provide further evidence for the lateral segregation of the mitochondrion/bacteria main lipid components, we have carried out a combined thermodynamic and morphological study of Langmuir−Blodgett films made by PE−CLP and PC−CLP lipid mixtures.

Langmuir−Blodgett films have been extensively used as model systems to mimic natural membranes and to provide information on lipid−lipid interactions.[16,17] Moreover, this technique allows the system to confine interactions within a two-dimensional layer, thus avoiding mesophasic structural changes, occurring in three-dimensional model membrane systems and provides information relevant to the lateral organization of lipid domains. Lipid monolayers deposited onto solid substrates have been also widely employed to investigate domain formation by means of atomic force microscopy (AFM).[18,19]

In this paper, we have investigated the thermodynamic behavior of mixed monolayers of cardiolipin−dipalmitoylphosphatidylcholine (CLP−DPPC) and cardiolipin−dipalmitoylphosphatidylethanolammine (CLP−DPPE), studying their Langmuir surface pressure and surface potential isotherms, at different cardiolipin molar fractions. The use of fully unsaturated CLP and fully saturated DPPC and DPPE justifies these monolayers as a simple model of a mitochondrial membrane, where the

[†] Universita' di Roma "La Sapienza".
[‡] Universita' di Roma "Tor Vergata".
* To whom correspondence should be addressed.

10.1021/jp051893q CCC: $30.25
Published on Web 08/02/2005

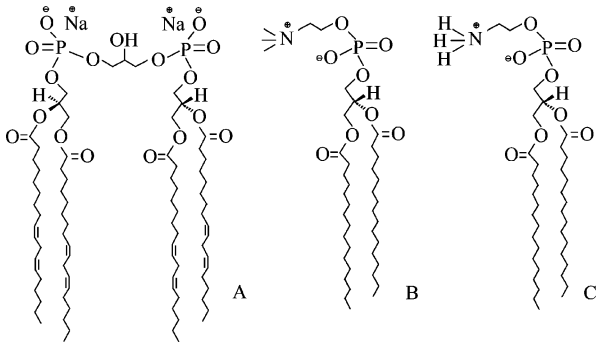

Figure 1. Chemical structure of the three lipids employed: (A) cardiolipin, (B) DPPC, (C) DPPE.

phospholipid saturated acyl chains range between 45 and 55%.[20] Simultaneous measurements of surface pressure and surface potential vs molecular area allows us to correlate directly the variation of thermodynamic stability to the changes in dipole moment organization at varying molecular packing, underlining the interactions governing the lipid miscibility. Mixed monolayers deposited onto mica were structurally characterized by an innovative "needle-sensor" AFM technique by means of which images of the surface morphology can be obtained without the direct contact with the surface and the disadvantages of tip-to-sample touching, but with an increased sensitivity in comparison to the "noncontact" mode. Our results indicate the presence of a cardiolipin arrangement in CLP−DPPE monolayers composed of separated regions of DPPE and CLP−DPPE mixture with a well-defined stoichiometric composition. Such an arrangement does not appear in the mixed CLP−DPPC monolayers.

The fact that the phase-separated morphology is tunable with lipid content points to the possibility that the cell can attain a desired surface geometry by regulating the lipid composition of its membrane. It has recently been shown[21] that for a binary lipid mixture in the gel−fluid coexistence region, the morphology of the gel aggregates can be compact (isolated domains) or branched, depending on the relative lipid content. The compact aggregates form isolated domains, while the branched ones form a network that enables membrane compartmentalization on a nanometer scale. Moreover, there is increasing evidence that domains with definite lipid composition are present in different biological membranes,[9,10] and the formation of stoichiometric complexes of different membrane lipids to attain optimal packing has been suggested.[22] The formation of a regular arrangement of these complexes ("superlattice") at a definite "critical" composition, driven by sterical and/or dipolar interaction between the polar heads, could represent a possible mechanism to induce lateral separation alternative or complemental to liquid crystalline/gel phase separation driven by tail ordering.

2. Experimental Section

2.1. Materials. Cardiolipin (CLP), dipalmitoylphosphatidylcholine (DPPC), and dipalmitoylphosphatidylethanolammine (DPPE) were obtained by Sigma Chemical Co. and were used without further purification. The chemical structures of the three lipids employed in this study are shown in Figure 1. We used CLP with purity >99%, a saturated/unsaturated ratio of 0.01, and chains of the same length within 96%. The melting temperature of DPPC, DPPE, and CLP are 42, 63, and about 19 °C, respectively. Lipids were dissolved at appropriate concentration in chloroform or in a mixture of chloroform and methanol (5:1 vol:vol). In all experiments, the subphase was 0.1 M NaCl, prepared using Milli-Q grade deionized water (Millipore). The pH of the subphase was routinely measured before each deposition. Its value was pH = 6.2 ± 0.2. In this pH range, both DPPC and DPPE can be assumed neutral or weakly negatively charged. All chemicals were analytical grade (Merck).

2.2. Measurements of Monolayer Surface Pressure. Mixed CLP/DPPC and CLP/DPPE monolayers with different molar fractions were prepared at the air−water interface according to the Langmuir technique.[16] Surface tension measurements were carried out by means of the Wilhelmy plate technique with the trough (MINITROUGH, KSV, Finland) enclosed in a Plexiglas box to reduce surface contamination. Appropriate amounts of the lipid solution were spread by a microsyringe onto the aqueous subphase; after the deposition, the solvent was allowed to evaporate for 10 min before beginning the compression. Symmetric compression was achieved with two moving barriers at a constant rate of 10 mm min^{-1}.

All measurements have been performed at the temperature of 25.0 ± 0.2 °C. No precaution to prevent oxidation was taken, but we ascertained that the reproducibility of the surface pressure, at the same area per molecule, in different experimental conditions, was within ±2 mN/m. Results reported here represent average values on three different isotherms, at least.

It is well-known that exposure of unsaturated lipids to air can result in changes in the surface pressure and/or miscibility transition pressure in lipid monolayers.[23] These effects can be softened by completing experiments quickly, since significant changes in surface pressure are observed after several minutes of exposure to air.[24] In our case, times were optimized by completing the data acquisition of an isotherm or a deposition cycle in roughly 10 min. Moreover, to allow comparison of different samples, the procedure was standardized, so that each sample was exposed for the same time to air. Once deposited, the supported monolayers to be observed by AFM (see section 2.4) were kept under vacuum.

2.3. Measurements of Monolayer Surface Potential. Surface potential measurements were performed using the noncontact, nondestructive, vibrating plate capacitor method, originally introduced by Kelvin and improved by Yamins and Zisman.[25−27] We used a computer-controlled device (SPOT1, KSV), with a 17 mm diameter active electrode, placed at less than 3 mm above the air−water interface and a stainless steel reference electrode immersed in the subphase.

The surface pressure and the surface potential were measured simultaneously during the film compression; at the beginning of each experiment, the surface potential of the aqueous phase was measured, and this value was assumed as reference. Before compression, a sufficiently long waiting time to allow for the complete evaporation of the solvent was required for a good stabilization of the initial value of the potential.

We adjusted the probe parameter setting in order to reduce to a negligible extent the stray capacitance effect due to the small variation of the electrode distance from the interface, in different measurements. The reproducibility of the surface potential was within ±10 mV.

2.4. Atomic Force Microscopy. Supported monolayers used in AFM measurements were first deposited on a water subphase at the temperature of 25 °C and then transferred onto freshly cleaved mica substrate, at two different surface pressures, at 7 and 35 mN m^{-1}. Langmuir−Blodgett monolayers are stable over a long period of time if stored in a dry atmosphere.

Experiments were performed both in air and in ultrahigh vacuum, using a noncontact needle-sensor AFM from Omicron

(Taunusstein, Germany). The probe consists of a long, thin needle cemented onto the front of a quartz rod oscillated by a 1 MHz generator.[28] The needle, oscillating with a magnitude of a few nanometers at a distance of ~10 nm from the sample, is influenced by the gradient of either lateral or vertical forces. As a result, resonance parameters such as amplitude, frequency, and phase shift of the quartz oscillator may change, and discrimination of phase shift between the generator and the oscillator provides the required signal for AFM. The needle-sensor AFM operates like a tapping mode AFM; because of the vertical oscillation, it experiences gradient of attractive and repulsive force without real contact with the sample surface and the disadvantage of tip-to-sample touching (contact mode). Measurements were carried out in constant phase-shift mode; the tip is moved back and forth to maintain a constant phase-shift value, and the resulting image provides the topography of the sample (the height *z*). The typical lateral resolution is of the order of a few angstroms, similar to the one obtained in contact mode or in tapping mode. However, in this case, because of the characteristics of the biological samples employed, we obtained a lateral resolution of the order of a few nanometers. Vertical resolution is typically higher, so that variations in the order of a few angstroms can be appreciated.

3. Results

3.1. Thermodynamic Analysis. The surface pressure vs area isotherms of pure CLP, DPPC, DPPE, and mixed CLP−DPPC and CLP−DPPE monolayers at the air−water interface are shown in Figures 2 and 3A.

DPPC monolayer shows the typical transition occurring around 8−10 mN m^{-1}, generally referred to liquid expanded to liquid condensed phase transition.[29] Pure CLP and DPPE monolayers exhibit, at the same temperature, isotherms characteristic of a single phase. The isotherms for the mixed CLP−DPPC and CLP−DPPE films fall between those of the pure lipid monolayers. The progressive decrease of CLP molar fraction, from 1 (pure CLP film) to 0.4, results in a gradual shift of the isotherm toward smaller molecular areas, without affecting the overall curve shape. No differences between mixed CLP−DPPC and CLP−DPPE isotherms are observed within this CLP molar fraction interval. On the other hand, when CLP molar fraction decreases below 0.4, a different behavior is observed depending on the presence of DPPC or DPPE. The CLP−DPPC mixed films undergo a gradual increase of collapse pressure upon increasing DPPC molar fraction, from ~48 mN m^{-1}, which is the collapse pressure for pure CLP, up to 73 mN m^{-1}, where pure DPPC collapse is observed (Figure 2 A), indicating a complete miscibility between the two components, in agreement with previously reported values[30,31] and with the recent results of Nichols-Smith et al.,[32] who observed complete miscibility for mixed cardiolipin Egg-PC monolayers at all the molar ratios. The fact that complete miscibility is observed both for pure DPPC (completely saturated hydrophobic chains) and for Egg-PC, whose hydrophobic tails are mainly unsaturated and of different length,[33] seems to rule out an exclusive role of the hydrophobic part in determining the miscibility of CLP and PC.

In CLP−DPPE films two distinct collapse pressures (48 and 53 mN m^{-1}) appear at CLP molar fraction lower than 0.4 (Figure 3A and Figure 4, where the collapse pressures for all the mixed monolayers are shown as a function of CLP molar fraction), indicating that the increase of DPPE concentration promotes the phase separation of the film in two components with a different degree of stability, the less stable one collapsing very close to the CLP collapse pressure. The comparison of these results, the phase separation observed in CLP−DPPE and the absence of such a separation in CLP−DPPC and in CLP−PC (with different saturated and unsaturated tails) mixed film, points out to a major role of polar heads interaction in determining the different behavior.

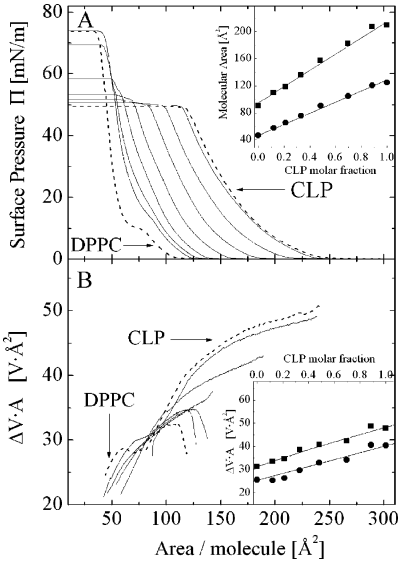

Figure 2. Surface pressure and dipole moment vs area per molecule isotherms for CLP (cardiolipin), DPPC, and mixed CLP−DPPC monolayers. The curves falling between those of the pure lipid monolayers refer to some selected different compositions varied from CLP−DPPC (0.9:0.1) to CLP−DPPC (0.15:0.85). Insets show molecular area and molecular Δ*VA* curves (parts A and B, respectively) as a function of the CLP composition, at 5 mN m^{-1} (■) and 45 mN m^{-1} (●) surface pressure; a continuous line is drawn to show the ideal behavior. The concentrations are expressed as mole fractions. The subphase is 0.1 M NaCl electrolyte solution. The temperature is fixed to the value 25 °C within 0.5 °C.

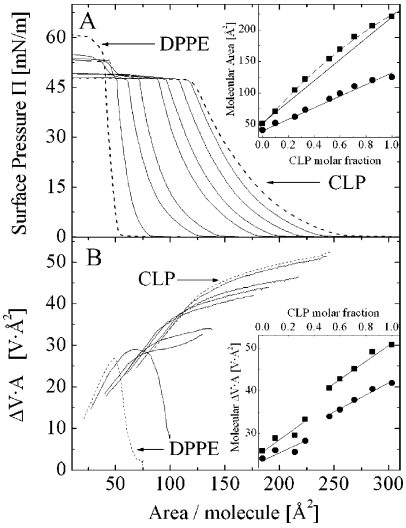

Figure 3. Surface pressure and dipole moment vs area per molecule isotherms for CLP (cardiolipin), DPPE, and mixed CLP−DPPE monolayers. The curves falling between those of the pure lipid monolayers refer to some selected different compositions varied from CLP−DPPE (0.85:0.15) to CLP−DPPE (0.1:0.9). Insets show molecular area and molecular Δ*VA* curves (parts A and B, respectively) as a function of the CLP composition, at 5 mN m^{-1} (■) and 45 mN m^{-1} (●); dashed line represents a polynomial fit, and a continuous line is drawn to show the ideal behavior. The concentrations are expressed as mole fractions. The subphase is 0.1 M NaCl electrolyte solution. The temperature is fixed to the value 25 °C within 0.5 °C.

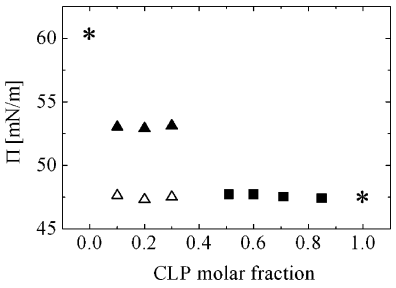

Figure 4. Values of collapse pressure of mixed CLP−DPPE monolayers as a function of CLP molar fraction. For CLP molar fraction higher than 0.4, a single collapse pressure is observed at 48 mN m^{-1} (■). For CLP molar fraction lower than 0.4, the system experiences two distinct collapse pressures, at 52−53 mN m^{-1} (▲) and at 47−48 mN m^{-1} (△). Collapse pressures of pure DPPE and CLP components are also shown (∗), at 60 and 47 mN m^{-1}, respectively.

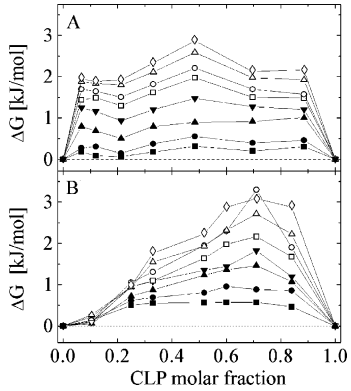

Figure 5. Excess free energy of mixing Δ*G* of mixed CLP−DPPC (A) and mixed CLP−DPPE (B) monolayers as a function of CLP composition, calculated at different surface pressure: (■) 5, (●) 10, (▲) 15, (▼) 20, (□) 25, (○) 30, (△) 35, and (◇) 40 mN m^{-1}. The horizontal dashed line is drawn to guide the eye only. Errors in Δ*G* derived from the surface-molecular area integration have been quoted to be within some percent.

The miscibility of CLP and DPPC or DPPE can be analyzed in terms of the excess free energy of mixing Δ*G* for the two systems[34] upon integration of the surface pressure−area (Π−*A*) isotherms, from zero to different values of the surface pressure, according to the expression

$$\Delta G = \int_0^{\Pi} (A_{12} - X_1 A_1 - X_2 A_2)\, \mathrm{d}\Pi \qquad (1)$$

where A_i and X_i are the area per molecule and the molar fraction of component *i*, respectively, and A_{12} is the area per molecule in the mixture. In the absence of any interaction between the components, $\Delta G = 0$. Deviations from an ideal behavior results in $\Delta G < 0$ (attractive interactions) or in $\Delta G > 0$ (repulsive interactions), providing information on whether the interaction is energetically favored or not.

The excess free energy Δ*G* for CLP−DPPC and CLP−DPPE mixtures at the investigated molar ratios, from 5 to 40 mN m^{-1}, is shown in Figure 5. At high CLP molar fractions, a large positive excess free energy of mixing, indicative of repulsive interactions between the components, is observed for both the mixed monolayers. At lower CLP content, Δ*G* for CLP−DPPC films remains positive (Figure 5A), while Δ*G* approaches zero for CLP−DPPE films (Figure 5B) as expected for an ideal system.

The "overall effective dipole" Δ*VA* for mixed CLP−DPPC and CLP−DPPE films as a function of the area *A* per molecule is reported in Figures 2 and 3B, respectively. Δ*V* represents the difference between the electric surface potential values measured in the monolayer-covered and in the monolayer-free (before spreading) subphase and is related to the dipole moment of the molecules forming the film through the Helmholtz equation:[35]

$$\Delta V = \frac{\mu_N}{A\epsilon_0\epsilon_r} + \Psi_0 \qquad (2)$$

where ϵ_r is the "effective" dielectric constant within the layer and ϵ_0 is the permittivity of free space, μ_N is the normal component of the molecular dipole moment, *A* is the area occupied by each molecule, and Ψ_0 is the double-layer contribution. Since at high ionic strength the double-layer contribution Ψ_0 is relatively small[36] and its value is not strongly dependent on the surface pressure, the quantity Δ*VA*, as an approximate measure of the normal component of the dipole moment, is plotted in Figures 2 and 3B. The shape of these curves for mixed CLP−DPPC and CLP−DPPE films changes smoothly from pure CLP to pure DPPC or pure DPPE.

To better understand the mixing behavior of the film, the Π vs *A* and Δ*VA* vs *A* isotherms have been analyzed to extract the "partial molecular area" and "partial molecular dipole moment" at definite surface pressure values.[37] These quantities, shown for example in Figure 6 for the CLP−DPPE system, can be obtained from the measured Π vs *A* and Δ*VA* vs *A* isotherms by means of the tangent method.[38,39] In the case of mixed CLP−DPPC monolayers no deviation from linearity is observed for all the surface pressures investigated (inset of Figure 2A,B). Correspondly, the partial dipole moment curves of CLP and DPPC do not show any variation from values corresponding to the pure CLP and DPPC components (data not shown).

Molecular area curves for mixed CLP−DPPE monolayers (inset of Figure 3A) show statistically significant positive deviations from linearity at surface pressure of 5 mN m^{-1} (squares) and 35 mN/m (data not shown for clarity of presentation); next to CLP collapse, at surface pressure of 45 mN m^{-1} (circles), no appreciable deviation from linearity is observed, probably due to the high degree of compression which forces a closest molecular packing. Positive deviation from linearity in the molecular area of "mixed molecule" corresponds to values of the partial area for each component higher than that in the pure film, indicative of a nonideal mixing behavior (see Figure 6, left, A). On the other hand, the linear dependence of the molecular area observed at 45 mN m^{-1} surface pressure indicates ideal mixing behavior. In agreement, the values of partial molecular area remain constant and equal to the value of pure components (Figure 6, left, B). In other words, each CLP and DPPE molecule occupies the same area in mixed and in pure monolayers.

More interestingly, the molecular dipole moment at the various surface pressures (inset in Figure 3B) can be only fitted by two distinct straight lines, and a sharp discontinuity in the mixing behavior can be observed close to 0.33 CLP molar fraction, providing evidence for an effect depending on CLP molar fraction. In fact, at all the surface pressures investigated, the value of the partial dipole moment is strongly reduced with respect to that in pure film when CLP mole fraction is lower than 0.4 (Figure 6, right). This result is indicative of a dipolar interaction among CLP and DPPE molecules, which is not observed in CLP−DPPC films. The effect disappears at CLP molar fraction higher than 0.4, where CLP dipole moment reaches the value of the pure monolayer. In similar mixed monolayers this behavior has been interpreted as due to the occurrence of a well-defined, stoichiometric, molecular packing,

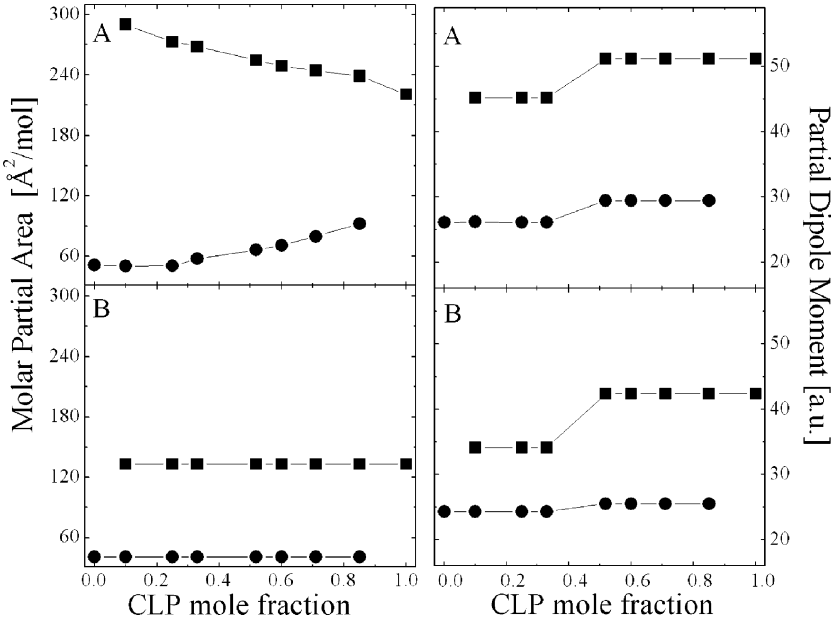

Figure 6. Partial molecular area and partial molecular Δ*VA* for CLP (■) and DPPE (●) as a function of composition calculated at a surface pressure of (A) 5 and (B) 45 mN m^{-1}. Note the sharp variation of dipole moment values after CLP 0.33 molar fraction.

with dipoles of the different molecular species arranged to screen effectively each other.[19,39]

The occurrence of this screening effect at a well-defined CLP molar fraction (close to 0.33 molar fraction), corresponding to a 1:2 molecular ratio, suggests the formation of a specific "optimal" molecular arrangement, involving two DPPE molecules for each CLP molecule. At CLP excess, where the stoichiometric complexes are diluted in a CLP richer phase, the screening effect is not any longer observed.

3.2. AFM Measurements. The topology of mixed CLP−DPPE monolayers deposited onto mica at the pressure of 7 mN m^{-1} for 0.3, 0.2, and 0.1 CLP molar fraction and at the pressure of 35 mN m^{-1} for the 0.2 CLP molar fraction is shown in Figures 7 and 8, respectively. We have reported images with a relatively small magnification (15 and 10 μm frames) to show the largest view of the sample. For comparison, we show a typical topology of a CLP−DPPC monolayer deposited at the pressure of 7 mN m^{-1} for a 0.2 CPL molar fraction in Figure 9.

To increase the definition of the structures and the borders of the domains, the monolayer surface topology has been acquired from the phase-shift signal, which is proportional to the first derivative of the height *z*. Typical line profiles through the images are shown in the insets of Figures 7 and 8. The AFM images of CLP−DPPC monolayers, in the same experimental conditions, show a rather uniform surface roughness, excluding the presence of any domain distribution (Figure 9). Images of samples deposited at 7 mN m^{-1} with 0.3 CLP molar fraction reveal circular flat domains systematically higher than the surrounding grainy phase (Figure 7A). These domains are regular in shape and varying in size from 1 to 2 μm. Decreasing CLP molar fraction down to 0.2 (Figure 7B), the dimension of the flat domains increases up to about 5 μm diameter, maintaining the same morphology. At the smallest CLP fraction investigated, the flat, elevated domains occupy most of the monolayer surface, and they change their shape: large and irregular regions extend through the whole frame, while the grainy matrix is now confined in small area randomly sprinkled in the flat regions (Figure 7C). For comparison with biological membranes the study of the monolayers at higher surface pressure is usually considered more relevant.[40] At higher surface lateral pressure, when the film is more compacted, the difference in height between the less ordered CLP-rich domains and the more compacted DPPE domains becomes smaller and the contrast decreases. At pressures higher than 40 mN m^{-1}, domains are difficult to recognize. The same overall behavior is observed for films deposited at surface pressure of 35 mN m^{-1}, as shown in Figure 8 for the 0.2 CLP molar fraction.

The increase of the area of the elevated domains upon increasing the DPPE concentration suggests that they are mainly formed by DPPE molecules. This hypothesis is also supported by the fact that saturated DPPE can undergo to a more ordered organization when compared to the unsaturated CPL molecules, providing a rational for the higher height of the flat domains. Evaluation of the area occupied by domains and grainy matrices in samples at different compositions (see Table 1, $(D/G)_{exp}$) does not correspond to that calculated from the CLP−DPPE molar fraction, simply taking into account the effective molecular area of the two pure components, as evaluated from the isotherms (see Table 1, $(D/G)_{calc}$).

This result can be rationalized considering that the grainy phase is composed by DPPE and CLP while the flat one almost exclusively by DPPE molecules. This picture coming from AFM images is also in agreement with the CLP−DPPE isotherm results obtained by LB measurements. The less stable phase, collapsing close to 48 mN/m, can be attributed in fact to the grainy phase while the most stable one, collapsing to a value close the one of the pure DPPE, can be attributed to the DPPE flat domains (Figure 3A).

Under these hypotheses, the surface of the different microdomains can be quantitatively evaluated considering that the areas occupied by the domains (*D*) and by the grainy phase (*G*) are related by the following equation:

$$\frac{D}{G} = \frac{A_{DPPE}}{A_G}\frac{(N_{DPPE} - fN_{CLP})}{(N_{CLP} + fN_{CLP})} = \frac{A_{DPPE}}{A_G}\frac{(X_{DPPE} - fX_{CLP})}{X_{CLP}(1+f)} \quad (3)$$

where A_{DPPE} and A_G are the area of the molecular entities present in the domains and in the grainy phase; N_{CLP} and N_{DPPE},

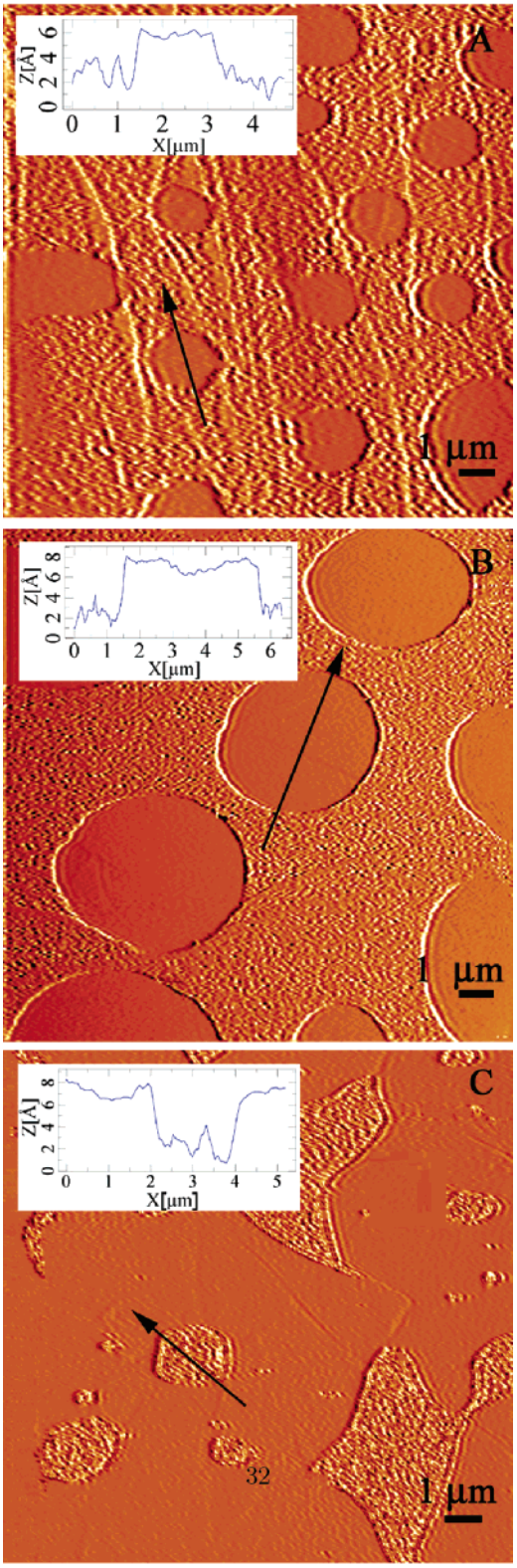

Figure 7. AFM images relative to CLP-DPPE samples at CLP molar fraction of (A) 0.3, (B) 0.2, and (C) 0.1, at surface pressure $\Pi = 7$ mN m^{-1}. The arrows indicate the direction of the profiles reported in the insets. Frame dimension is 15 μm; bars represent 1 μm.

$X_{CLP} = N_{CLP}/(N_{CLP} + N_{DPPE})$, and $X_{DPPE} = 1 - X_{CLP}$ are the number and the molar fraction of CLP and DPPE molecules, respectively. The parameter f is the fraction of DPPE molecules present in the grainy phase ($f = 0$ corresponds to separated regions of DPPE and CLP domains).

The evaluation of the parameter f requires the knowledge of the area A_{DPPE} and A_G, at the two surface pressures investigated

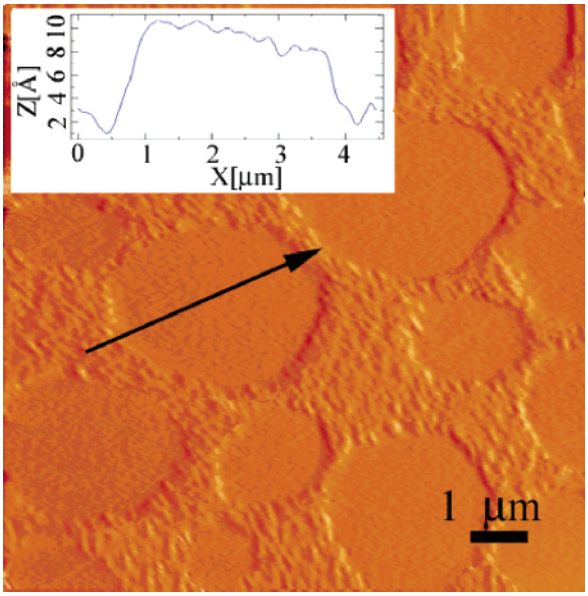

Figure 8. AFM images relative to CLP−DPPE sample at CLP molar fraction of 0.2, at surface pressure $\Pi = 35$ mN m^{-1}. The arrow indicates the direction of the profiles reported in the insets. Frame dimension is 10 μm; bar represents 1 μm.

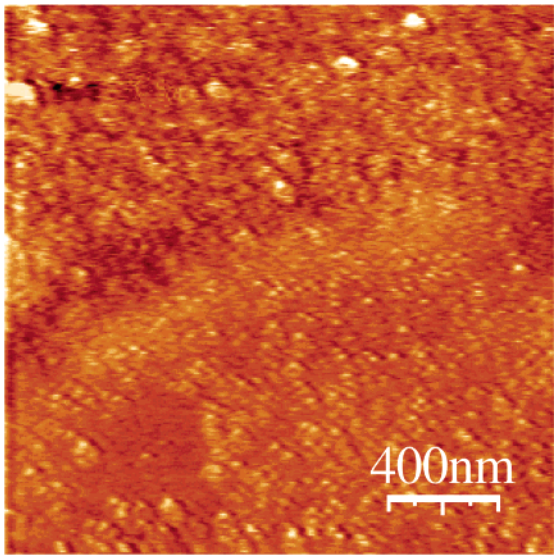

Figure 9. A typical AFM image relative to CLP−DPPC sample at CLP molar fraction of 0.2, at the surface pressure of $\Pi = 7$ mN m^{-1}. The observed roughness does not reveal any apparent structure, the rms amplitude of the profiles being approximately within 1.5 Å. Bar represents 400 nm.

(7 and 35 mN m^{-1}). A_{DPPE} is directly measured from the corresponding (Π−A) isotherms (Figure 3A). A_G has been estimated from the width ΔA_0 of the plateau of the first collapse occurring in the isotherms at CLP molar fraction less than 0.4. After the normalization $\Delta A = \Delta A_0(A_{CLP}/A_{CLP}^{collapse})$, required to take into account that measurements have been performed at pressures different from that of collapse, the following relation holds:

$$A_G = \frac{\Delta A}{(1+f)X_{CLP}} \quad (4)$$

From the above analysis, by measuring the ratio D/G from the AFM images, $((D/G)_{exp}$ in Table 1), we obtain a value of f very close to $f = 2$ for all the mixed films at all the investigated surface pressures (Table 1).

TABLE 1: Analysis of the Area of the DPPE Domains (D) and DPPE−CLP Grainy Phase (G) Obtained from AFM Images and (Π−*A*) Isotherms at Different CLP Molar Fractions (*X*) at Two Surface Pressures (7 and 35 mN m^{-1})[a]

Π [mN m^{-1}]	CLP *X*	$(D/G)_{calc}$	$(D/G)_{exp}$	Δ*A* [Å^2]	f
	0.1	2.1 ± 0.01	5.2 ± 0.3	6.5 ± 0.3	2.1 ± 0.2
7	0.2	0.96 ± 0.04	0.81 ± 0.04	22 ± 1	1.9 ± 0.2
	0.3	0.55 ± 0.02	0.17 ± 0.01	31 ± 2	2.0 ± 0.2
35	0.2	1.24 ± 0.05	1.08 ± 0.04	13.0 ± 0.6	2.1 ± 0.2

[a] $(D/G)_{calc}$ has been evaluated on the basis of the film composition, assuming two separate regions for DPPE and CLP. $(D/G)_{exp}$ has been calculated from the measured area of the domains in the AFM images. *f* is obtained from eq 3.

Following these results, a intermixing between CLP and DPPE (grainy phase) is possible only for a mole ratio less than 0.2. At this value, an optimum molecular structure consisting of two DPPE molecules per one CLP molecule is achieved. At higher DPPE content, DPPE molecules in excess with respect to the DPPE/CLP ratio of 0.2 tend to separate as a pure DPPE phase, and that in AFM images appears as the flat higher domains.

4. Discussion

We report herein an investigation on the biophysical behavior of monolayers made with the three main components of the mitochondrion inner membrane, namely phosphatidylcholine, phosphatidylethanolamine, and cardiolipin. The results indicate that for the mixed CLP−DPPC monolayers the overall thermodynamic behavior is independent of mole fraction, while for CLP−DPPE monolayers, a critical fraction exists above which DPPE molecules segregate in definite domains. This investigation has been carried out by means of "standard" lipids, i.e., the completely saturated DPPC and DPPE and the unsaturated CLP. Thus, the composition of our monolayers does not exactly reproduce that of the mitochondrion membrane; nevertheless, our data unambiguously demonstrate that the nature of the phospholipid polar head is the first determinant in the modulation of the interaction with the strongly charged CLP phospholipid.

In fact, although DPPC and DPPE have identical saturated chains, the occurrence of well-defined domains is observed only in the presence of DPPE. This finding rules out that domains are simply due to the liquid crystalline−gel phase separation induced by the presence of two components having transition temperature above and below the temperature at which the investigation has been carried out.

When the CLP molar fraction is lower than 0.4, a phase separation is evidenced by the surface-pressure curves of CLP−DPPE monolayers, showing two distinct collapses (Figures 3A and 4); moreover, at the same CLP molar ratios, the value of the partial molecular dipole moment is strongly reduced (Figure 6, right), suggesting a screening effect due to the formation of a complex among CLP and DPPE molecules. If domains were simply due to different melting temperatures, the domain-covered surface should increase monotonically without the "threshold" behavior. The optimal lateral packing of the lipids occurs in fact only at definite "critical" compositions, while deviations from this composition lead to the coexistence of domains formed by the component in excess, i.e, DPPE. In line, DPPE domain formation in CLP−DPPE monolayers occurs only above a mole ratio of 0.2, as demonstrated by AFM images (Figures 7 and 8).

Taken together, our data indicate that, in mixed monolayers, CLP interacts in a different way with DPPE and DPPC. In the case of DPPC−CLP monolayers, our analysis indicates a nonideal behavior between the components at each mole ratio that can be interpreted as indicative of the formation of a regular molecular arrangement or of a random one, as observed by Berclatz et al.[41,42]

On the other hand, quantitative analysis of the surface size of domains and matrix in AFM images of DPPE−CLP monolayers indicates the occurrence of a DPPE/CLP ratio $f = 2$, which suggests an hexagonal arrangement,[22] being the DPPE excess confined in the flat domains. A regular arrangement would be entropically favored because of the spacer action of each molecule in the mixed monolayers that decreases the crowding among similar molecules at the headgroup level, making the head rotation easier. This favorable effect is maximum in a regular distribution, where the rotations and vibrations of the elements are less hindered than in less organized systems. In conclusion, we propose that in mixed monolayers of CLP−DPPE the optimal lateral arrangements and minimum packing frustration of the components are achieved assuming a conformation resulting in a fixed DPPE−CLP molar ratio, corresponding to $f = 2$.

The hypothesis that in mixed monolayers CLP and DPPE adopt a regular arrangement, rather than a random one, can be related to the lipid lateral organization in biological membrane. The existence of particular lipid arrangements in plasma membrane has been repeatedly emphasized, and both experimental and theoretical data indicate that membranes are not laterally homogeneous but are made by domains with a distinct composition.[8,43,44] Recently, increasing evidences of the presence of domains with definite lipid composition have been also reported in other biological membranes.[9,10] A proposed mechanism of domain formation in cell membranes is the "phase separation" of lipid species, resulting from the lipid−lipid and the lipid−protein interactions.[8] However, the role of lipid phase separation in the establishment and maintenance of domains in biological membrane is still under debate.[45] The observation that lipid components in biological membranes are able to segregate also in model membranes suggests that lipid−lipid interaction plays a key role in the lateral membrane organization, also in vivo. Our data on the domain formation in monolayers composed by DPPE and CLP, two main components of mitochondrion membranes, indicate that a definite stoichiometric ratio gives rise to lateral segregation of a lipid species such as observed in gangliosides−phospholipid and sphingolipid−phospholipid membrane systems.[19,39]

References and Notes

(1) Schlame, M.; Rua, D.; Greenberg, M. L. *Prog. Lipid Res.* **2000**, *39*, 257−288.

(2) Hostetler, K. V.; van den Bosch, H. *Biochim. Biophys. Acta* **1972**, *260*, 380−386.

(3) Torok, Z.; Demel, R. A.; Leenhouts, J. M.; de Kruijff, B. *Biochemistry* **1994**, *33*, 5589−5594.

(4) Jiang, F.; Ryan, M. T.; Schlame, M.; Zhao, M.; Gu, Z.; Klingenberg, M.; Pfanner, N.; Greenberg, M. L. *J. Biol. Chem.* **2000**, *275*, 22387−22394.

(5) Choi, S.; Swanson, J. M. *Biophys Chem* **1995**, *54*, 271−278.

(6) Zamzami, N.; Kroemer, G. *Curr. Biol.* **2003**, *13*, 671−735.

(7) Kuwana, T.; Mackey, M. R.; Perkins, G.; Ellisman, M. H.; Latterich, M.; Schneiter, R.; Green, D.; Newmeyer, D. *Cell* **2002**, *111*, 331−342.

(8) Simons, K.; Ikonen, E. *Nature (London)* **1997**, *387*, 569−572.

(9) Mileykovskaya, E.; Dowhan, W. *J. Bacteriol.* **2000**, *182*, 1172−1175.

(10) Kaway, F.; Shoda, M.; Harashima, R.; Sadaie, Y.; Matsumoto, K. *J. Bacteriol.* **2004**, *186*, 1475−1483.

(11) Wang, X.; Bogdanov, M.; Dowhan, W. *EMBO J.* **2002**, *21*, 5673−5681.

(12) Zhang, W.; Bogdanov, M.; Pi, J.; Pittard, A. J.; Dowhan, W. *J. Biol. Chem.* **2003**, *278*, 50128−50135.

(13) Sonnino, S.; Cantu, L.; Acquotti, D.; Corti, M.; Tettamanti, G. *Chem. Phys. Lipids* **1990**, *52*, 231−241.
(14) Brocca, P.; Bernardi, A.; Raimondi, L.; Sonnino, S. *Glicocony J.* **2000**, *17*, 283−299.
(15) Yuan, C.; Johston, L. J. *Biophys. J.* **2001**, *81*, 1059−1069.
(16) Roberts, G. *Langmuir−Blodgett Films*; Plenum Press: New York, 1990.
(17) Dynarowicz-Latka, P.; Dhanabalan, A.; Olivera Jr., O. N. *Adv. Colloid Interface Sci.* **2001**, *91*, 221−293.
(18) Dufrene, Y. F.; Lee, G. L. *Biochim. Biophys. Acta* **2000**, *1509*, 14−41.
(19) Diociaiuti, M.; Ruspantini, I.; Giordani, C.; Bordi, F.; Chistolini, P. *Biophys. J.* **2004**, *86*, 321−328.
(20) Ardail, D.; Privat, J. P.; Egret-Charlier, M.; Levrat, C.; Lerme, F.; Louisot, P. *J. Biol. Chem.* **1990**, *265*, 18797−802.
(21) Muresan, A. S.; Diamant, H.; Lee, K. *J. Am. Chem. Soc.* **2001**, *123*, 6951−6952.
(22) Virtanen, J. A.; Cheng, K. H.; Somerharjus, P. *Proc. Natl. Acad. Sci. U.S.A.* **1998**, *95*, 4964−4969.
(23) Lai, C. C.; Tang, S. H.; Finlayson-Pitts, J. *Langmuir* **1994**, *10*, 4637−4644.
(24) Stottrup, B. J.; Stevens, D. S.; Keller, S. L. *Biophys. J.* **2005**, *88*, 269−276.
(25) Yamins, H. G.; Zisman, W. A. *J. Chem. Phys.* **1933**, *1*, 656−661.
(26) Gaines, G. L. *Insoluble Monolayers at Liquid−Air Interface*; Interscience: New York, 1966.
(27) Brockman, H. *Chem. Phys. Lipids* **1994**, *73*, 57−79.
(28) Bartzke, K.; Antrack, T.; Fchmidt, K. H.; Damman, E.; Schatterny, C. H. *Int. J. Optoele.* **1993**, *8*, 669−676.
(29) Lyklema, J. *Fundamentals of Interface and Colloid Science*; Academic Press: New York, 2000; Vol. III.
(30) Nicolay, K.; Sautereau, A. M.; Tocanne, J. F.; Brasseur, R.; Huart, P.; Ruysschaert, J. M.; de Kruijff, B. *Biochim. Biophys. Acta* **1988**, *940*, 197-208.
(31) Luckham, P.; Wood, J.; Froggatt, S.; Swart, R. *J. Colloid Interface Sci.* **1993**, *156*, 164−172.
(32) Nichols-Smith, S.; Teh, S.-Y.; Kuhl, T. L. *Biochim. Biophys. Acta* **2004**, *1663*, 82−88.
(33) Ochi, H.; susumu, T.; Kajiyama, G. *Biochem. J.* **1996**, *318*, 139−144.
(34) Goodrich, F. C. *Proc. Second Int. Congress Surface Activity*; Butterworth: London, 1957; Vol. 1.
(35) Taylor, D. M. *Adv. Colloid Interface Sci.* **2000**, *87*, 183−203.
(36) Israelachvili, J. N. *Intermolecular and Surface Forces*, 2nd ed.; Academic Press: London, 1992.
(37) Chattoray, D. K.; Birdi, K. S. *Adsorption and the Gibbs Surface Excess*; Plenum Press: New York, 1984.
(38) Atkins, P. W. *Physical Chemistry*; Oxford University Press: London, 1990.
(39) Maggio, B.; Ariga, T.; Calderon, R. O.; Yu, R. K. *Chem. Phys. Lipids* **1997**, *90*, 1−10.
(40) Koberl, M.; Hinz, H. J.; Rapp, G. *Chem. Phys. Lipids* **1997**, *85*, 23−43.
(41) Berclatz, T.; McConnell, H. M. *Biochemistry* **1981**, *20*, 6635−6640.
(42) Berclatz, T.; Geoffroy, M. *Biochemistry* **1984**, *23*, 4033−4039.
(43) Brown, R. E. *J. Cell Sci.* **1998**, *11*, 1−9.
(44) Rietveld, A.; Simons, K. *Biochim. Biophys. Acta* **1998**, *1376*, 467−479.
(45) Munro, S. *Cell* **2003**, *115*, 377−388.